Appendix to Bindi et al., Soil Dynamics and Earthquake Engineering, 2012

Seismic hazard assessment in Central Asia: outcomes from a site approach

D. Bindi , K. Abdrakhmatov , S. Parolai , M. Mucciarelli , G. Grünthal , A. Ischuk , N. Mikhailova , J. Zschau

Data set

The set of felt intensities at each site is completed using virtual intensities (D'Amico and Albarello, 2008). To this aim, the Intensity Prediction Equation developed for Central Asia (Bindi et al., 2011b) using the same macroseismic catalog are applied to the seismic catalog collected within CASRI project and composed by about 8400 earthquakes with hypocentral depth less than 40 km (Figure 3). Except for few earthquakes with magnitude <3.5, the magnitude range covered by the catalog is from 3.5 to 8.3 (see histogram in Figure 3). Most of the earthquakes with magnitude larger than 7 (green circles) occurred along the northern Tien-Shan (between Kazakhstan and Kyrgyzstan) and the South-Hissar fault zone (Tajikistan). In particular, a sequence of strong earthquakes occurred along the Chou-Kemin-Chilik fault zone including the 1887, M 7.3 Verny earthquake, the 1889, M 8.3 Chilik earthquake, the 1911, M 8.2 Kemin earhthquake and 1938, M 6.9 Kemin-Chou earthquake (e.g. Delvaux et al., 2001; Kalmetieva et al., 2009). Other strong earthquakes occurred in the Chatkal-Fergana (north-western Kyrgyzstan) seismic zone (1946, M=7.5 Chatkal earthquake; Kalmetieva et al., 2009); in southern Tien-Shan (e.g 1949, M=7.6 Khait earthquake) (Evans et al., 2009); in northern Pamir (1974, M=7.4 Markansu earthquake; Jackson et al., 1979; Langston and Dermengian, 1981); along the border between Tajikistan and Uzbekistan, in the South Gissar source zone (1907, M=7.3 Karatog earthquake; Babaev et al., 2005); in the Pamir area (1911, Sarez M=7.4 earthquake; Babaev et al., 2005). Among the most recent ones, the data set includes the Ms=7.3, 1992 Suusamyr earthquake (Mellors et al., 1997; Ghose et al., 1997), occurred in Kyrgyzstan (northern Tien-Shan), in a region located north-east of the Talas-Fergana fault. The seismic catalog is mainly covering the period 1800-2005 but about 70 earthquakes occurred earlier are also included . Figure 4 shows the cumulative number of earthquakes against time, counting separately earthquakes with magnitude smaller and larger than 5.5. The curve for magnitude >=5.5 shows an almost regular increase with time starting from 1880 while the trend for M<5.5 shows three main slope changes. The first two changes (around 1920 and 1960) correspond to periods of significant improvements in the seismic monitoring of Central Asia, with the installation of local networks. The decrease of the rate after 1990 is related to the collapse of the Soviet Union that led to a general worsening of the local network monitoring in Central Asia due to the lack of financial support for maintaining the stations and updating the networks. The annual rate is summarized by the Gutemberg-Richter distribution shown in the bottom panel of Figure 4. A least square fit considering the model y=a+bM provided the values a=5.61-0.89M, being the 95% confidence bounds for parameters a and b equal to (5.46, 5.77) and (0.87, 0.92), respectively. Finally, examples of felt histories for four large towns in Central Asia are shown in Figure 5, considering both observed (red) and virtual (black) intensities. The largest intensities are generally associated to observed data

points while the virtual data points improve significantly the distribution of intensities smaller than V.

Reliability assessment

To assess the robustness of the hazard estimates at different sites, we repeat the hazard computations but adding to each time history one further intensity value corresponding to a hypothetic earthquake occurred today. In particular, we carry out the test as follow:

1) we add to each location a hypothetic intensity relevant to a fake earthquake occurring today. We created three modified data sets, corresponding to added intensities equal to VII, VIII, and IX;

2) we compute the hazard for the original data set (p_0) and for the modified one (p_{new}) considering as threshold the intensity value equal to the added one. We then compare the two probabilities estimated for each case. The comparison is performed selecting those localities with p_0 of exceeding the selected intensity in a 50 year period greater than 0.05.

Figure C shows the difference between the hazard estimates computed for the modified site history and for the original one, normalized to this last. In general, the relative differences are very small (e.g. for I=VII about 90% of points show a relative differences smaller than 10%). This indicated that the available time histories allow to perform robust estimates. The differences are generally positive, that is the hypothetical intensity has been added after an elapsed time from the last observation shorter than the expected return period for that intensity. Then, the occurrence of the added intensity is not probable accordingly to the return period estimated from the catalog (see for example the results close to the epicentral area of 1992 Suusamyr earthquake, whose location is shown in Figure 1 of Bindi et al, SDEE paper). More interesting are the negative differences, which indicate a seismic drought longer than the average return period estimated for that intensity from the catalogue. For locations where the difference is negative, the seismic history at the site could be less representative for evaluating the hazard. Figure D shows that some positive differences are obtained for intensity VII and VIII, but small in absolute value. The results are summarized in Figure 10, where the cumulative distribution functions (CDF) of the relative difference for the three considered intensities are shown. The asymmetry of the CDFs is due to the fact that shorter inter-event times (IET) are more probable that longer ones even if no Poissonian assumption is made: the strong monotonically decreasing trend of IET combined with the decreasing frequency distribution of intensity is in fact driving the sharp decrease of hazard shown in Figure C.

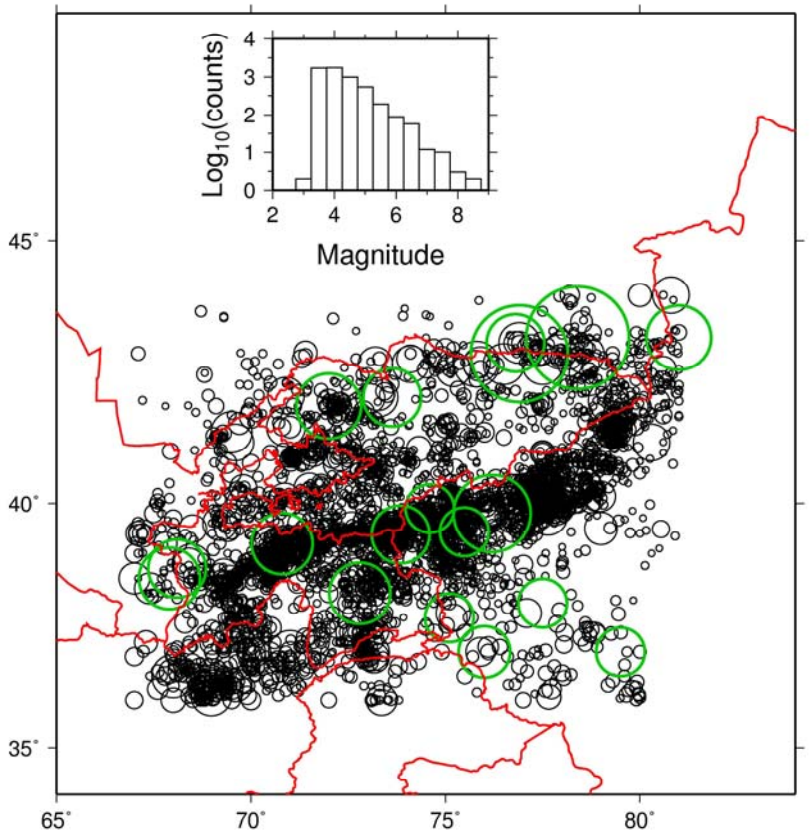

Figure A Distribution of the epicenters (black circles with dimension proportional to magnitude) of the earthquakes used to complete the felt histories by using a intensity prediction equation. Green circles indicate earthquake with M>7. In the inset, the distribution of the magnitude values is also shown.

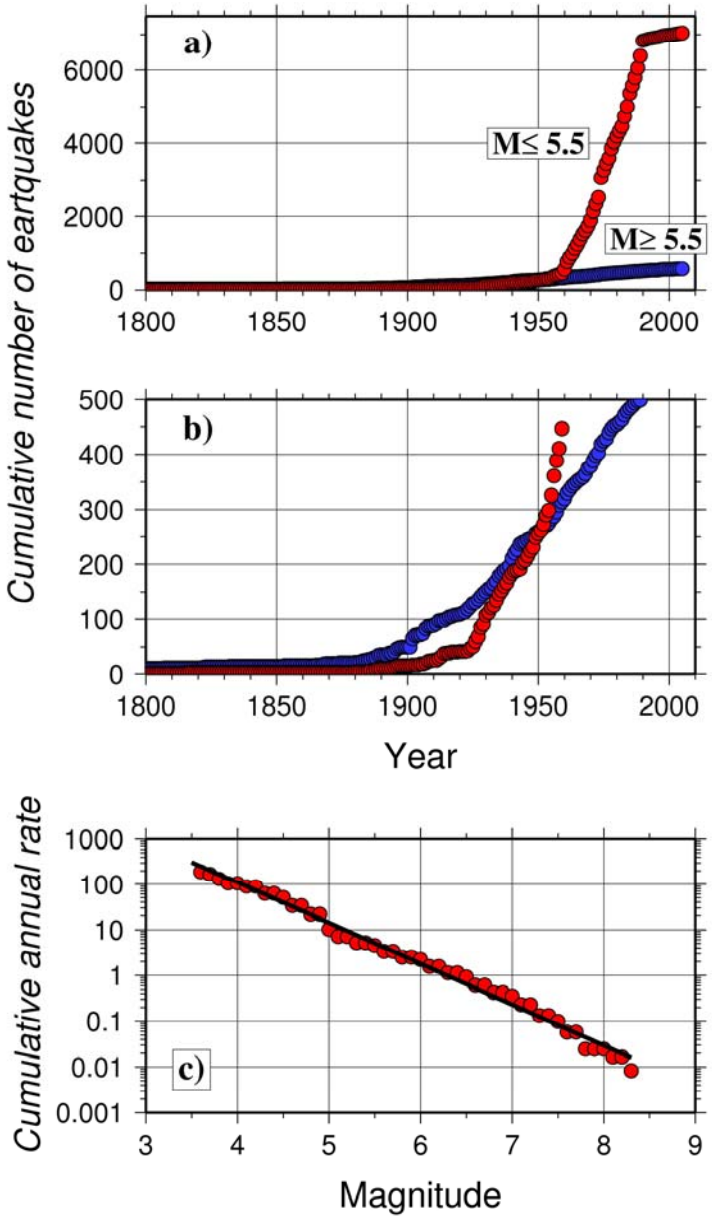

Figure B Top. Culumative number of earthquakes with magnitude larger (blue) and smaller (red) than 5.5. Middle: the same as in the top panel but zooming on the y-scale. Bottom. Cumulative annual rate computed for the considered catalog (red) and bet fit exponential model (black line).

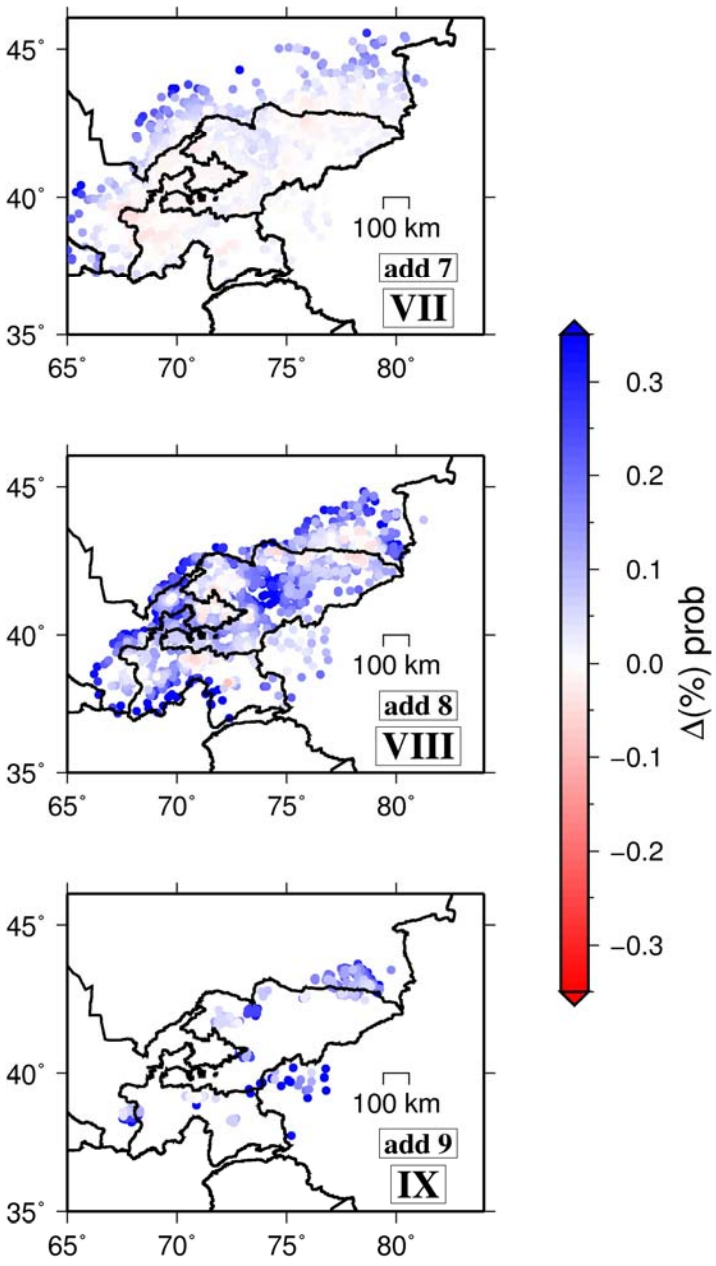

Figure C. Top: Locations characterized by a probability of exceeding (p_0) for I=VII in 50 years larger than 0.05. The color scale measures the difference between the probability of exceedance (p_{new}) computed after adding an intensity I=VII to each seismic history and p_0, being the difference normalized to p_0. Middle: the same as in the top panel but computing the probability for I=VIII for both the original data set and the one obtained after adding I=VIII to the seismic histories. Bottom: the same as in the middle panel but for I=IX.

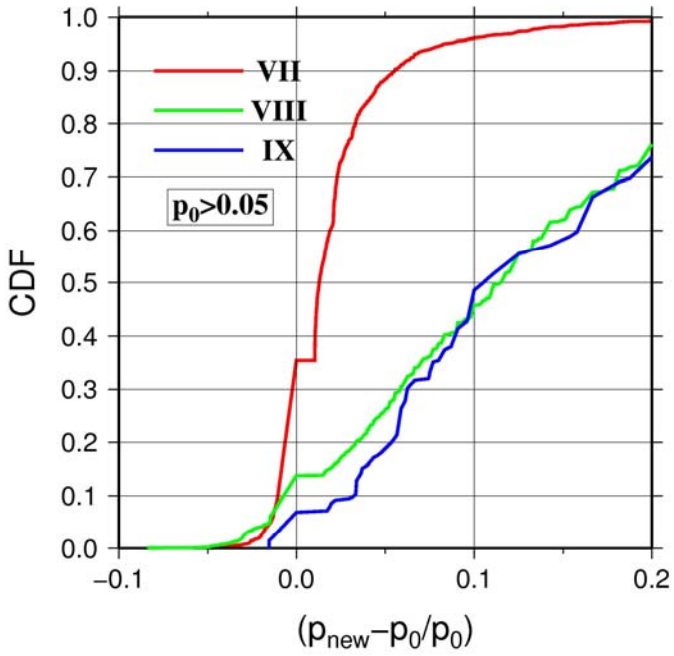

Figure D. Cumulative distribution functions (CDFs) relevant to the probability distributions shown in Figure 7. The curves for I=VII, VIII, and IX are shown with different colors as indicated in the legend.